World Conference on Timber Engineering Oslo 2023

PLASTIC DEFORMATION CONTRIBUTIONS OF CLT AND LTF SHEAR WALLS: DEVELOPMENT OF AN ANALYTICAL CAPACITY MODEL

Angelo Aloisio[1], Yuri De Santis[1], Francesco Boggian[2], Massimo Fragiacomo[1], Roberto Tomasi[3]

ABSTRACT: This paper compares the experimental cyclic response of Cross-Laminated Timber and Light Timber Frame shear walls. The goal is extracting the fractions of the lateral displacement due to sliding, panel's deformation and rocking. The three contributions to the total displacement, expressed in percentage, are then used to develop an analytical capacity model valid for CLT and LTF shear walls. The model is based on the sole equilibrium equations of the hold-down forces, obtained by reducing the pivot length of the hold downs reactions. Additionally, they examine the overstrength of the CLT panel, and LTF sheathing to the shear walls collapse due to the hold-down failure.

KEYWORDS: Experimental cyclic response; timber engineering; shear walls; rocking; Cross Laminated Timber; Light Timber Frame.

1 INTRODUCTION

Currently, the most diffuse timber constructive systems in Europe are based on the use of Light Timber Frame (LTF) and Cross Laminated Timber (CLT) shear walls [1]–[3]. There are numerous and diverse capacity models in the scientific literature for Cross-Laminated Timber (CLT) and Light Timber Frame (LTF) shear walls. Some researches merely attempt to elaborate closed-form models which best seize the observed response. Others, like [4], append to the mentioned efforts, an interpretative framework useful in developing simplified and reliable tools for the prediction of the lateral response. Specifically, [4] developed an analytical procedure and a simplified numerical model for the elastic response of LTF and CLT shear walls. They found that, in the elastic response range of CLT shear walls, 77% of the total displacement is due to rigid-body rotation, 16% to the rigid-body translation and 7% to the panel deformation. Conversely, in LTF shear walls, 45% is expected to the rigid-body rotation, 6% to the rigid body translation, and 45% and 4% to the sheathing-to-framing connection and sheathing panel deformation, respectively. In this paper, the authors investigate CLT and LTF systems in the post-elastic range. The rigor and straightforwardness of elastic analysis vanishes when dissipative phenomena arise. The authors devoted their efforts in interpreting experimental data by clustering the displacement response in rocking, sliding and deformation components. In a second step, based on the observed results, an elementary capacity model based on the sole hold-down experimental response is compared to the experimental results to estimate the related approximation.

2 EXPERIMENTAL TESTS

The results presented in this paper descend from the experimental data on LTF and CLT shear wall tests performed at the University of Trento. [5]–[7]. The first part of this paper focuses on the description of the test setup and the experimental responses. The second part attempts to understand the leading deformation contributes to the shear walls lateral response and proposes a capacity model based on the hold-down contribution. The research novelty of this paper, with respect to [6], [8], derives from the (1) complete report of the cyclic test results on CLT shear walls, (2) comparing CLT and LTF by decomposing the experimental response into rocking, sliding and deformation fractions, (3) the proposal of a novel capacity model driven by hold-down reactions, and (4) the estimation of overstrength factors.
The full description of the test setup of LTF and CLT shear walls is detailed in [5], [9], [10]. Tab.2 summaries the primary outcomes of the cyclic tests. Tab.2 reports only F_u and v_u, F_u measuring the strength capacity, while v_u the displacement capacity. The former expresses ultimate resistance; the latter is related to ductility. The optimum performance of a structural system derives from the optimum balance between resistance and ductility. Therefore, F_u and v_u may be suitable synthetic indicators of the experimental structural performance. Fig.2 presents the results in the form of force-displacement curves.

[1] Department of Civil, Construction-Architectural and Environmental Engineering Università degli Studi dell' Aquila, L'Aquila, 67100, Italy (angelo.aloisio1@univaq.it; yuri.desantis@univaq.it; massimo.fragiacomo@univaq.it)
[2] Department of Civil, Environmental and Mechanical Engineering, University of Trento, Trento , Italy (francesco.boggian@unitn.it)
[3] Faculty of Science and Technology , Norwegian University of Life Sciences, Ås , Norway (roberto.tomasi@nmbu.no)

https://doi.org/10.52202/069179-0263

Table 1: *Cyclic test result of LTF shear walls: Fu, ultimate experimental racking load; vu, slip corresponding to the ultimate load; both evaluated according to EN12512*

	LTF	
Test	F_u [kN]	v_u [mm]
STD-L0	47.6	60.6
STD-L10	58.1	78.4
STD-L20	57.5	74.5
2F-L20	38.9	33.5
150-L20	49.6	70.8
50/RG-L20	97.6	76.0
50-L20	65.5	53.5
SCREW-L20	57.6	74.9
WHD-L10	34.0	54.1

Table 2: *Cyclic test result of CLT shear walls: Fu, ultimate experimental racking load; vu, slip corresponding to the ultimate load; both evaluated according to EN12512*

	CLT	
Test	F_u [kN]	v_u [mm]
STD-L0	55.6	42.2
STD-L20	80.2	43.3
NA620-L0	124.0	29.1
NA620-L20	146.5	28.6
ND620-L0	132.9	30.4
ND620-L20	160.5	32.6
NA340-L20	83.6	57.4
NAWH-L20	66.6	57.7

3 EXTRACTION OF THE PLASTIC DEFORMATION COMPONENTS

The sliding fraction is estimated as the limit of the ratio between the horizontal displacements in points D and B, as illustrated in Fig.1:

$$s := \lim_{u_B \to \infty} \left| \frac{u_D(t)}{u_B(t)} \right| \quad (1)$$

The values of $u_D(t)$ and $u_B(t)$ are direct measures from the experimental campaign, and when plotted, they reveal an hyperbolic behaviour, with a clearly visible asymptote for higher values of the imposed displacement

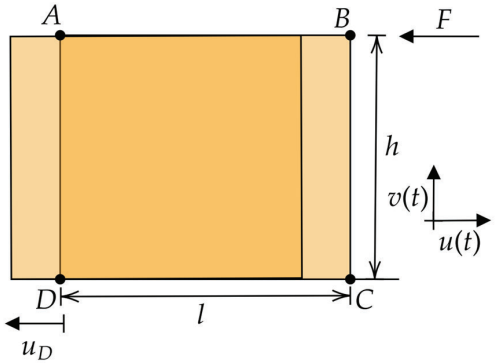

Figure 1*: Illustration of the rigid-body translation of the panel and the adopted notation.*

The relative displacement between the points A-C and B-D is a measure of the diagonal deformations in the East and West directions identified by d_E and d_W respectively. At this stage, the authors assume that the panel manifests a predominant shear deformation, as illustrated in Fig.2.

$$d_{E,W} = r_2 - r_1 \quad (2)$$

The shear displacement δ derives from Eq.(2) by expliciting the two radii r_2 and r_1:

$$\delta = l - \left[(h\sqrt{2} - d_{E,W})^2 - h^2 \right]^{0.5} \quad (3)$$

The ratio between δ and u_B approaches a constant value at higher displacement values. The following definition of the deformation fraction, d, attempts to grasp the approaching asymptot.

$$d := \lim_{u_B \to \infty} \left| \frac{\delta}{u_B} \right| \quad (4)$$

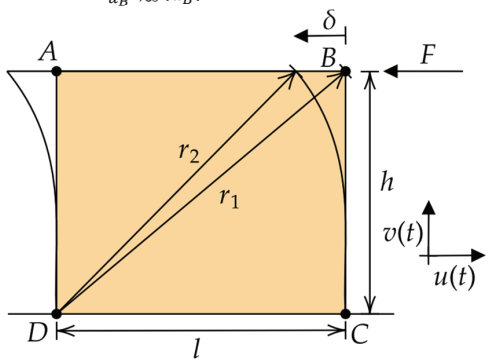

Figure 2*: Illustration of the shear deformation of the panel and the adopted notation.*

The rocking component is estimated as a complement to one of the already estimated sliding and deformation contributions, see Fig.3:

$$r = 1 - (s + d) \quad (5)$$

The whole displacement field of the shear wall is illustrated in Fig.7, where all the contribution to the top displacement u_B are highlighted: u_D represents the sliding contribution while δ represents the deformation contribution, both evaluated in the previous sections. The rocking component can be expressed by θh. By assuming small displacements, the displacements can be written as:

$$u_B - u_D - \delta = \theta h \quad (6)$$

$$v_C = \theta(l - x) \quad (7)$$

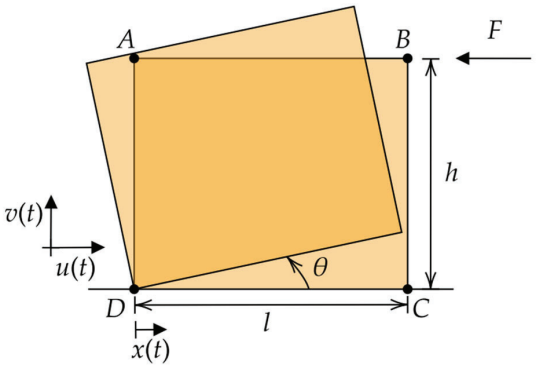

Figure 3 *Illustration of the rigid-body rotation of the panel and the adopted notation.*

https://doi.org/10.52202/069179-0263

4 RESULTS

Tab.3 reports the three displacement contributions in all the tested specimens, expressed as percentages. The displacement components in Tab.3 refer to the post-elastic behaviour. They originate from Eqs.(1),(4),(5) respectively, which present an asymptotic definition of the three displacement fractions. The experimental data reveal that the three displacement components rapidly converge towards a definite value after the elastic phase. The values stationarity proves that the excitation amplitude does not modify the balance between the three contributions after a certain post elastic displacement value.

Table 3: *The table attempts to synthesize the displacement components due to sliding, deformation and rocking, expressed as a fraction of the imposed displacement in point B, estimated using Eqs. (1),(4),(5) respectively.*

Test	s [%]	d [%]	r [%]
LTF STD-L0	9.5	4.7	85.9
LTF STD-L10	2.1	17.8	80.1
LTF STD-L20	5.1	21.7	73.2
LTF 2F-L20	3.8	33.4	62.8
LTF 150-L20	7.6	34.6	57.8
LTF 50/RG-L20	7.7	18.8	73.5
LTF 50-L20	0.8	15.4	83.9
LTF SCREW L20	2.0	34.5	63.5
LTF WHD-L10	1.4	8.1	90.5
CLT STD-L0	5.6	4.2	90.2
CLT STD-L20	5.0	12.8	82.3
CLT NA620-L0	7.7	3.8	88.5
CLT NA620-L20	3.6	7.9	88.6
CLT ND620-L0	4.0	8.6	87.4
CLT ND620-L20	8.5	5.7	85.8
CLT NA340-L20	4.1	2.2	93.7
CLT NAWH-L20	6.8	0.1	93.0

The prevalent contribution to the total displacement comes from the rigid-body rotation. The rocking motion of LTF shear walls is lower than CLT: LTF shear walls are more deformable than CLT. The vertical load has almost the same effects in both the shear walls: the load increment reduces the rocking component. The vertical load acts as a rotation restraint. The reduction of the base connections determines a significant increment of the rocking motion, like in the case without hold-downs (WHD). Interestingly the test LTF SCREW, which uses screws distributed uniformly on the bottom rail as a sliding restraint, shows that the presence of screws may influence the rocking mechanism, by offering an additional uplift restraint, thus limiting the rocking percentage as seen from Tab.3.

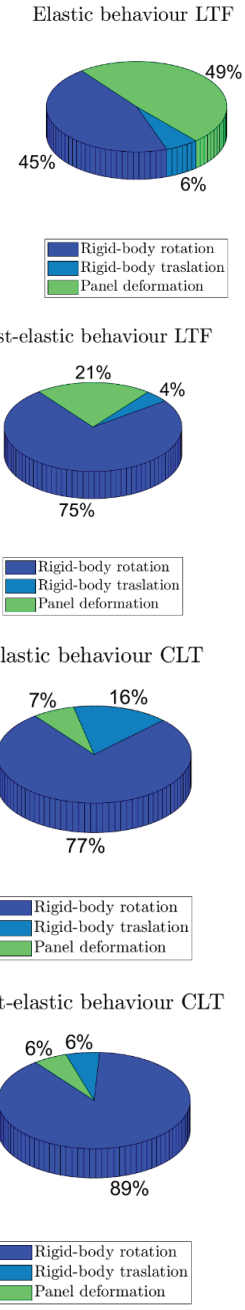

Figure 4*: Percentage of displacement on top of the shear walls due to each single contribution in both the elastic (calculated by* [4]*) and post-elastic range (as calculated from the experimental data. in this paper)..*

The sliding component does not significantly change between LTF and CLT shear walls. The rigid-body translation mainly depends on the transverse resistance of the base connections and does not likely depend on the vertical load. This shred of information conveys some details about the occurring of friction phenomena. The amount of the Coulomb-type friction restraint depends on the vertical load: the substantial independence of the

https://doi.org/10.52202/069179-0263

sliding fraction on the vertical load proves the possible independence of friction in the sliding restraints, primarily provided by the base connections. In the current setup, friction phenomena are then negligible compared to the restraining capacity of the connections.

Additionally, Tab.4 proves the substantial independence of the sliding component on the angle brackets. The CLT shear wall has four angle brackets, while the LTF shear wall has two. Nonetheless, the CLT sliding is lower than LTF. The sliding fractions are quite similar between the two structural typologies and the increment in the number of the angle brackets does not enhance the sliding restraint, likely. The panel deformation changes between LTF and CLT as expected. The impact of deformation on shear walls with low load values and a few base connections (WHD) is shallow and very similar between the two structural typologies. However, as the load increases as well as the base connections, the impact of deformation increases in LTF, while CLT does not deform significantly.

5 CAPACITY MODEL

The dominance of the rocking response due to the hold-downs deformation may inspire the proposal of an elementary capacity model based on the sole hold down reactions. However, the accuracy of the model mostly depends on an accurate estimation of the extension of the compressed area. In contrast with the elastic behaviour, the extension of the compressed area tends towards a sort of plastic asymptote due to the stress redistribution. The definition of the neutral axis is the following:

$$x_p := \lim_{u_B \to \infty} \left| l - \frac{v_C}{\theta} \right| \tag{8}$$

There are no studies about the trend of the stress in the compressed area, which depends on several factors: e.g. the planarity of contact areas, timber grading and the slenderness of the panel.

Tab.4 attests that the extension of the compressed area depends on the vertical load, the in-plane stiffness of the panel and the boundary restraints. The compressed area expands significantly when the vertical load raises, the in-plane stiffness reduces, and there are fewer base connections. An analytical correlation between the x_p variable and the three mentioned variables (vertical load, in-plane stiffness and boundary conditions) is critical for a conservative estimation of forces acting on the base connections. Specifically, the estimation of the pivot point is essential when assessing the force on the hold-downs: the assumption of the pivot point by one edge of the panel would significantly underestimate the hold-down reactions.

Table 4: *Estimate of the asymptotic neutral axis in the considered test configurations.*

Test	$\mathbf{x_p}$ [m]	$\mathbf{x_p/l}$ [%]	**r** [%]
LTF STD-L0	0.01	0.4	85.9
LTF STD-L10	0.43	17.2	80.1
LTF STD-L20	0.71	28.2	73.2
LTF 2F-L20	0.72	28.8	62.8
LTF 150-L20	0.02	0.8	57.8
LTF 50/RG-L20	0.01	0.4	73.5
LTF 50-L20	0.01	0.4	83.9
LTF SCREW L20	0.59	23.7	63.5
LTF WHD-L10	0.09	3.6	90.5
CLT STD-L0	0.19	7.5	90.2
CLT STD-L20	0.88	35.4	82.3
CLT NA620-L0	0.20	8.0	88.5
CLT NA620-L20	0.13	5.3	88.6
CLT ND620-L0	0.05	2.0	87.4
CLT ND620-L20	0.70	27.9	85.8
CLT NA340-L20	0.37	14.9	93.7
CLT NAWH-L20	0.48	19.2	93.0

Tab.4 lists the expected extension of the compressed area. The second column presents the percentage ratio between the estimated x_p value and the base length l. The x_p extension depends on the balance between deformation and rocking components: the increment of the deformation fraction yields an increment of the x_p value. In this paper, the authors do not investigate the compressed area extension based on mechanical analytical models. This step would entail dedicated research efforts based on adequate mechanical models of the shear wall post-elastic response.

As shown in Fig.5, the wall is assumed to pivot around the position P of its neutral axis, characterized by a compression region of extension x_p; no specific assumption is made regarding the shape of the stress distribution in the compression zone. The contribution of angle brackets to the racking mechanism is neglected. Hereafter follows the equilibrium equations:

$$\uparrow \quad -ql - H + k_C \sigma_C x_p t_{\text{eff}} = 0 \tag{9}$$

$$\circlearrowleft \; Fh - ql\left(\frac{l}{2} - x_p\right) - H(l - x_p) + k_C \sigma_C x_p t_{\text{eff}} l_c = 0 \tag{10}$$

where q is the distributed vertical load, l the wall length, F the top horizontal force, h the wall height, H the hold down reaction force, σ_c the averaged compression stress on timber, k_c a modification parameter which accounts for the increment of resistance due to compression hardening and the shape feature of the stress diagram, x_p the extension of the neutral axis, t_{eff} is the thickness of the wall reacting in compression, l_c is the lever arm of the compression region. The k_c and the l_c factors are in fact unknown.

https://doi.org/10.52202/069179-0263

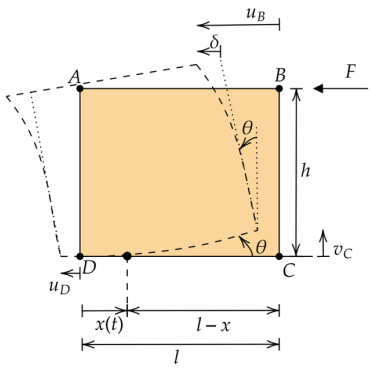

***Figure 5**: Mechanical model of the shear wall.*

The goal of this section is to demonstrate that the cyclic behaviour of the tested shear walls is mainly dependent on the hold-down. The force acting on the wall is then evaluated by considering the sole hold-down contribution to the rotational equilibrium, and neglecting the contribution of the unknown compression stresses in timber:

$$F = H \cdot \frac{\tau \cdot l}{h} + q \cdot \frac{l}{h}\left(\tau \cdot l - \frac{l}{2}\right) \quad | \quad \tau = \frac{l - x_p}{l} \tag{11}$$

Eq.(11) bestows the top horizontal force acting on the wall, given the hold-down force H, the vertical load q and the position of the pivot point x_p. The authors validated this model by comparing, in terms of cyclic curves and maximum force values, the forces measured in point B of the shear wall, with the horizontal force $F(t)$. $F(t)$ is obtained from the simplified model in Eq.(11), using the forces measured on the hold-downs $H(t)$ and the pivot point x_p value estimated in Tab.4. Tab.5 quantifies the discrepancies between the two curves in terms of the maximum forces.

***Table 5:** Comparison between the maximum forces in kN attained by the experimental cyclic tests and the capacity model based on the sole hold-down reactions.*

Test	$F_{max,exp}$	$F_{max,sim}$	Err. [%]
LTF STD-L0	72.8	75.9	-4.3
LTF STD-L10	75.6	82.7	-9.3
LTF STD-L20	75.6	68.1	10.0
LTF 2F-L20	60.0	54.6	9.0
LTF 150-L20	62.7	65.9	-5.2
LTF 50/RG-L20	128.9	116.1	9.9
LTF 50-L20	84.4	89.0	-5.4
LTF SCREW L20	74.2	74.7	-0.6
	Avg |Error|		6.7
CLT STD-L0	81.3	87.9	-8.1
CLT STD-L20	107.6	105.5	1.9
CLT NA620-L0	131.1	144.9	-10.5
CLT NA620-L20	143.6	149.5	-4.2
CLT ND620-L0	138.8	151.6	-9.2
CLT NDS20-L20	165.2	148.7	10.0
CLT NA340-L20	107.5	98.4	8.5
	Avg |Error|		7.5

Tab.5 proves that a capacity model based on the sole hold down reaction is quite faithful, and an elementary formula for the prediction of the hold-down response could descend by taking the 95% percentile of a Gaussian distribution of the τ factor in Eq.(11). Accurately, the 95% percentiles of the τ factor in the LTF and CLT shear walls are:

$$\begin{aligned} \tau_{\mathrm{LTF},95\%} &= 0.81 \\ \tau_{\mathrm{CLT},95\%} &= 0.86 \end{aligned} \tag{12}$$

These values suggest that the estimate of F needs a proper reduction of the pivot point of the hold-downs. The decrease is higher in the case of LTF shear walls due to the higher deformability. Eqs.(11)-(12) represent simplified formulations possibly useful for engineering purposes, which attempts to avoid underestimating the hold-down reaction by reducing the distance of the rotation point. In conclusion, LTF and CLT shear walls do not display significant differences in the considered configurations. This fact is essentially due to the overstrength of the panel to the base resistance derived from the base connections. Fig.6 illustrates the probability distributions of two resisting mechanisms: the failure reached during testing, mainly due to hold-down collapse, and the OSB sheathing/CLT panel collapse.

Fig.6 illustrates the probability distributions of two resisting mechanisms: the failure reached during testing, mainly due to hold-down collapse, and the OSB sheathing/CLT panel collapse.
The experimental probability density functions of the CLT and LTF shear walls are calculated directly from the values of failure of the cyclic tests. The probability density functions related to the capacity of the CLT panel / OSB sheathings derive by assuming the same variance of the corresponding experimental curves, and by assuming the shear failure of the OSB sheathing in LTF walls and the in-plane torsional shear failure in CLT panels (see [11], [12]). The authors used the following values of strength: $f_{vk} = 6.8$ MPa for OSB/3 and $f_{v,\mathrm{tor},k} = 2.5$ MPa for CLT [13], [14]. Fig.6 expresses the true nature of the considered structural systems. The two systems behave likewise due to the similarity of the base connections. Still, the CLT panel is far more resistant than the LTF when different boundary restraints and loads may activate other resisting mechanisms.

$$\gamma_{RD} = \frac{R_{k,b}}{R_{k,d}} \tag{13}$$

The authors reported the overstrength values, estimated as shown in Eq.(13). $R_{k,b}$ is the characteristic load bearing

capacity of the panel assuming the timber failure mode (brittle), while $R_{k,d}$ the characteristic load bearing capacity of the panel assuming the hold-down failure mode (ductile). The characteristic values are set equal to the 5-th percentile of the corresponding strength distributions. In the considered cases, the overstrength of LTF shear walls is almost two times of that of CLT. The obtained overstrength values are not general and depend from the specific structural configurations and the considered failure modes. The extension of these results to different structural arrangements must be the object of devoted efforts by the authors.

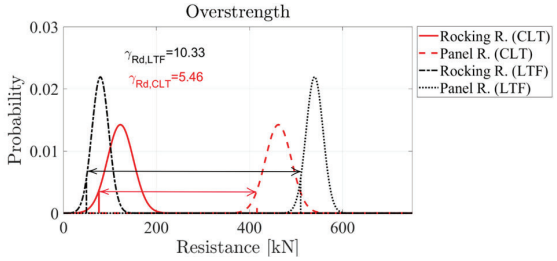

Figure 6: *Comparison between the experimental cyclic response of CLT shear walls and the capacity model based on Hold-Down measured forces.*

6 CONCLUSIONS

Light Timber Frame (LTF) and Cross Laminated Timber (CLT) shear walls exhibit similar response under cyclic loading. The authors compared the experimental test of LTF and CLT wall assemblies characterised by similar geometric features. The rigid-body rotation is the predominant deformation contribution. This contribution, expressed in percentage to the total deformation, is on average 75% and 88% in LTF and CLT specimens, respectively. The rocking response dominance, due to the hold-down deformation contribution, led to an elementary capacity model based on the hold down reactions and the assumption of a pivot point. The 95^{th} percentile of the Gaussian probability distribution of the ratio between the extension of the compressed area and the panel length is about 0.2: the adoption of the panel edge as a rotation point would determine an approximate 20% underestimation of the hold down reactions in the considered capacity model.

ACKNOWLEDGEMENT

The authors acknowledge the research efforts of Paolo Grossi, Paolo Endrizzi, Tiziano Sartori and Ermanno Acler, who carried out the experimental tests with the support of the staff of the University of Trento.

REFERENCES

[1] A. Aloisio, D. Pasca, R. Tomasi, and M. Fragiacomo, Dynamic identification and model updating of an eight-storey CLT building, *Eng. Struct.*, vol. 213, Jun. 2020, doi: 10.1016/j.engstruct.2020.110593.

[2] M. Piazza, R. Tomasi, and R. Modena, Strutture in legno, *Mater. Calc. e Progett. Second. le nuove Norm. Eur. (Wooden Struct. Mater. Calc. Des. Accord. to new Eur. Regul. Bibl. Tec. Hoepli Milano, Milano*, pp. 512–558, 2005.

[3] A. Aloisio, R. Alaggio, and M. Fragiacomo, Equivalent Viscous Damping of Cross-Laminated Timber Structural Archetypes, *J. Struct. Eng.*, vol. 147, no. 4, p. 4021012, 2021.

[4] D. Casagrande, S. Rossi, R. Tomasi, and G. Mischi, A predictive analytical model for the elasto-plastic behaviour of a light timber-frame shear-wall, *Constr. Build. Mater.*, vol. 102, pp. 1113–1126, 2016.

[5] P. Grossi, T. Sartori, and R. Tomasi, Tests on timber frame walls under in-plane forces: part 1, *Proc. Inst. Civ. Eng. Build.*, vol. 168, no. 11, pp. 826–839, 2015.

[6] E. Acler, P. Endrizzi, and R. Tomasi, Monotonic and cyclic in-plane behavior of CLT panels tested by using different types of metal devices, 2012.

[7] M. Andreolli and R. Tomasi, Bemessung von Gebäuden in Brettsperrholzbauweise unter Erdbebenbeanspruchung, *Bautechnik*, 2016.

[8] P. Grossi, PARETI INTELAIATE IN LEGNO: indagine sul comportamento meccanico tramite prove sperimentali a scala reale, University of Trento, 2011.

[9] P. Endrizzi, I sistemi di connessione di base del pannello xlam compensato di tavole indagine sperimentale in scala reale e modellazione numerica della capacità portante globale di parete ottenuta con l'impiego di una nuova tipologia di angolare a taglio, University of Trento, 2011.

[10] A. Aloisio, F. Boggian, T. Roberto, and M. Fragiacomo, The role of the hold-down in the capacity model of CLT andLTF shear walls based on the experimental lateral response, *Constr. Build. Mater.*, vol. In press, 2021.

[11] R. Tomasi, T. Sartori, D. Casagrande, and M. Piazza, Shaking table testing of a full-scale prefabricated three-story timber-frame building, *J. Earthq. Eng.*, vol. 19, no. 3, pp. 505–534, 2015, doi: 10.1080/13632469.2014.974291.

[12] F. Boggian, M. Andreolli, and R. Tomasi, Cross Laminated Timber (CLT) beams loaded in plane: testing stiffness and shear strength, *Front. Built Environ.*, vol. 5, p. 58, 2019.

[13] EN 594:2011 Timber structures, Test methods - Racking strength and stiffness of timber frame wall panels, *BSI, London UK*, 2011.

[14] R. Brandner, G. Flatscher, A. Ringhofer, G. Schickhofer, and A. Thiel, Cross laminated timber (CLT): overview and development, *Eur. J. Wood Wood Prod.*, vol. 74, no. 3, pp. 331–351, 2016.

https://doi.org/10.52202/069179-0263